12-1979

Shallow Convection on Day 261 of GATE: Mesoscale Arcs

C. Warner
University of Virginia

J. Simpson
University of Virginia

D. W. Martin
University of Wisconsin-Madison

D. Suchman
University of Wisconsin-Madison

F. R. Mosher
University of Wisconsin-Madison, moshe774@erau.edu

See next page for additional authors

Scholarly Commons Citation

Warner, C., Simpson, J., Martin, D. W., Suchman, D., Mosher, F. R., & Reinking, R. F. (1979). Shallow Convection on Day 261 of GATE: Mesoscale Arcs. *Monthly Weather Review, 107*(12). https://doi.org/10.1175/1520-0493(1979)107<1617:SCODOG>2.0.CO;2

Shallow Convection on Day 261 of GATE: Mesoscale Arcs

C. WARNER AND J. SIMPSON[1]

University of Virginia, Charlottesville 22903

D. W. MARTIN, D. SUCHMAN AND F. R. MOSHER

University of Wisconsin, Madison 53706

R. F. REINKING

Boundary Layer Dynamics Group, NOAA/ERL, Boulder, CO 80303

(Manuscript received 11 June 1979, in final form 5 October 1979)

ABSTRACT

On 18 September 1974, a cloud cluster growing in the GATE ship array was examined using aircraft flying close to one another at different heights, the geostationary satellite SMS-1, and radar, rawinsonde and ship data, with a view to elucidating mechanisms of convection. In this paper we concentrate analysis on cloudy convection in the moist layer.

In and above southerly surface monsoon flow approaching the cluster, clouds indigenous to the moist layer took the form of rows of tiny cumulus, and of arcs of cumulus mediocris, with patterns different from those of deeper clouds. From satellite visible images, arcs were traced for periods exceeding 2 h. Airborne photography showed that the arcs were composed of many small clouds. Radar data showed that they originated after precipitation. Apparently, throughout their life cycle, they perpetuated the pattern of an initiating dense downdraft. Eventually they yielded isolated cumulus congestus, again bearing precipitation. Aircraft recorded the distribution of thermodynamic quantities and winds at altitudes within the mixed layer, and at 537 and 1067 m. These data indicated that the arcs persisted as mesoscale circulations driven by release of latent heat in the clouds, rather than being driven by the original density current at the surface. The cloudy circulations were vigorous near and above cloud base, becoming weaker upward through altitude 1 km. The entire mesoscale circulation systems were of horizontal scale roughly 40 km.

The mesoscale cloud patterns of the moist layer appeared to play a primary role in heat transfer upward within this layer, and contributed to the forcing of showering midtropospheric clouds.

1. Introduction

The Atlantic Tropical Experiment of the Global Atmospheric Research Program (GATE) was centered on an area near 8.5°N, 22.5°W during summer 1974. On 18 September 1974 (day 261) a growing cloud cluster was monitored using the satellite SMS-1, ships and aircraft. A preliminary synthesis of observations of this cluster was given by Warner *et al.* (1977). Suchman and Martin (1976) included data from day 261 in an assessment of wind measurements by satellite tracking of clouds, and Suchman *et al.* (1977) have given a preliminary description of the evolving circulation of the cluster. Warner and Austin (1978) have described statistical aspects of radar echoes of the cluster. As will be seen in Section 4, much of the shallow convection associated with the cluster was organized in a manner very different from the deep convection. It is the purpose here to describe the shallow convection in the lowest 2–3 km of the moist layer south of the cluster, which contained the surface monsoon air flowing northward toward the cluster. Warner *et al.* (1980) treat the deep convection. These papers are condensed from a detailed report (Warner *et al.*, 1978). A future treatment will show how the cluster, occurring in relatively undisturbed conditions, was related to activity on larger scales.

A major GATE objective is to assess the interactions of air motions on different scales. This paper documents interactions between clouds indigenous to the moist layer and clouds of the mid-troposphere, and describes related events in the subcloud layer. An attempt is made to assess the role of the moist layer clouds in vertical exchanges of energy. The paper is chiefly concerned with arcs; the reader may like first to inspect the final figure—a schematic.

[1] Present affiliation: Goddard Laboratory for Atmospheric Science, NASA, Greenbelt, MD 20771.

0027-0644/79/121617-19$08.75

TABLE 1. Times (GMT) of passage of the aircraft at the corners of the box circuit, defined by latitudes 8°34′ and 9°56′N, and longitudes 21°2′ and 22°23′W. (The north leg was flown from west to east, then east to west, in succession.)

Aircraft	Altitude (m)	Corner			
		D_1 (NE)	D_2 (SE)	D_3 (SW)	D_4 (NW)
Sabreliner (NCAR)	12500	1554	1607	1618	1631
US-C130 (NOAA)	5800	1341	1400–03	1422–24	1444–47
		1505–12			
		1721	1701–1645	1555–52	1533–31
DC-6 (NOAA)	1067	1343	1409–11	1436	1502–04
		1528–32			
		1727	1702–1659	1635	1608–1558
Electra (NCAR)	537 & 35	1342	1406–10	1433–37	1459–1502
		1524–28			
		1717	1654–52	1623–19	1555–52
UK-C130	238 & 52	1358	1421–25	1447–1501	1524–27
		1549–53			
		1751	1729–25	1703–1656	1633–16

Black (1978) shows satellite photographs of two arc patterns which he associates with large cumulus clouds. That in Black's Figs. 9 and 10 may have been similar in nature to the arcs described here. Black calls for coordination of satellite and ground-based data. Here we provide this, and obtain a view of the arcs as self-perpetuating mesoscale entities, arising from and bearing the pattern of an initiating cold air outflow concomitant with rainfall, and eventually yielding isolated cumulus congestus, again bearing rain.

After a brief description of sources of data in Section 2, a representative aerological sounding is shown in Section 3, and maps of both shallow and deep clouds in Section 4. Arc patterns in the moist layer are traced in Section 5; they showed persistence over 2 h. Aircraft traverses through arcs are examined in Section 6, aircraft soundings and surface conditions in Section 7 and turbulent fluxes in Section 8, to throw light on how the arcs persisted and on the nature of the air circulations associated with them. A summary is given in Section 9 and conclusions are drawn in Section 10.

2. Sources of data

a. Aircraft data

Five aircraft simultaneously boxed a square of side 150 km which encompassed towers of the cluster. The different aircraft and flight altitudes, and the times of passing the box corners, are given in Table 1. The first box circuit was accomplished between 1340 and 1550 GMT by three aircraft in the low-level moist layer (up to 2.3 km) and one at ~6 km, the second between 1550 and 1750 GMT with an additional aircraft at altitude 12.5 km. The aircraft measured thermodynamic and wind data. All but the lowest carried time-lapse movie cameras; cloud maps were made using the methods of Ronne (1959) and Warner (1978). Turbulent heat fluxes were obtained from a gust probe on the DC-6 (Bean *et al.*, 1976).

b. Satellite data

From the geostationary satellite SMS-1, visible and infrared images with resolution ~1 km and 8 km, respectively, were obtained every 15 min, and used for following cloud developments and obtaining winds by cloud tracking (Suchman and Martin, 1976).

c. Radar data

Precipitation echoes were recorded digitally by the 5 cm radar aboard the Canadian ship *Quadra*, situated near 9°3′N, 22°36.5′W. This radar, and the data, have been described by Warner and Austin (1978). A three-dimensional scan cycle was completed every 5 min except during the period 1448–1614 GMT.

d. Rawinsonde data

Soundings from ships of the GATE B and A/B scale arrays have been used in this study, in their original form as supplied by the Center for Experiment Design and Data Analysis (NOAA).

e. Ship data

Thermodynamic and wind data from the booms of the ships *Dallas* (at 8°32′N, 22°31′W) and *Oceanographer* (at 7°44′N, 22°14′W) were compared with the all-sky movies taken aboard these ships. Profiles from the *Dallas* boundary layer instrument system [(BLIS) Garstang *et al.*, 1977] were examined.

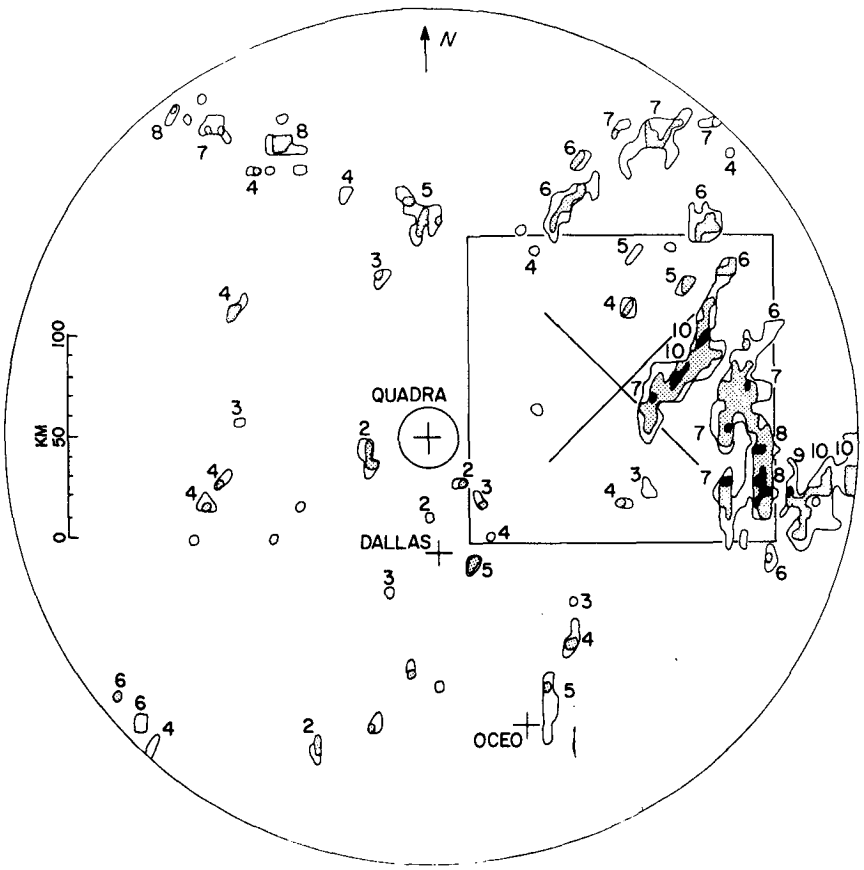

FIG. 1. 1629 GMT. Echoes from the *Quadra* radar, situated near 9°3'N, 22°36.5'W. Antenna elevation 0.35°. Maximum range 210 km. Minimum range 20 km (limited by clutter from the sea). Contours of reflectivity at the thresholds 16, 24 and 35 dB above 1 $mm^6 m^{-3}$ (dBZ)—equivalent to rainfall at about 0.3, 1.3 and 9 mm h^{-1}, measured by averaging over bins of area 18 km^2. The box was that flown by the aircraft. The cloud cluster was growing in the east half of the box. Digits refer to heights (km) of echo cores of reflectivity reaching 29 dBZ.

A radar view of the cluster, showing the positions of the aircraft circuit and of the ships, is given in Fig. 1.

3. A rawinsonde

The 1500 GMT *Oceanographer* sounding, shown in Fig. 2, appears to have been representative of undisturbed conditions southwest of the growing cluster, which was propagating slowly southwestward at ~2.5 m s^{-1}. In the sounding, several layers characteristic of the marine tropical atmosphere (Riehl, 1954) can be identified. The moist layer reached ~2.2 km. It contained a mixed layer of depth roughly 500 m. Surface winds at the *Oceanographer* reached 6–7 m s^{-1} from the south. The moist layer was capped by a stable layer, where the air was very dry and winds were light and from the northeast or east.

At ~4.5 km (600 hPa), the air was moist. In this humid layer the winds were northerly at ~6 m s^{-1}, and the stratification was conditionally unstable. There was a stable layer at 5 km. (There were many stratus and stratocumulus patches at ~2.5 and 5 km.)

Above 6 km the air was dry, with easterlies that persisted up to 8 km, at 7 m s^{-1} in this dry layer.

4. Cloud maps from the first circuit

The cloud maps shown in Fig. 3 were obtained using a 35 mm side camera on the US-C130 (with black and white film), and a 16 mm camera in the nose. The aircraft flew at ~130 m s^{-1}, and photographs were taken every 5 s (or ~650 m). Mapping was based chiefly on the C130 right side camera, and followed the method described by Ronne (1959). For an aircraft flying steadily past a cloud with a side-pointing cine-camera of constant frame rate, the range of the cloud is nearly proportional to the time or the number of frames of film required for it to pass across the field of view. If the position of

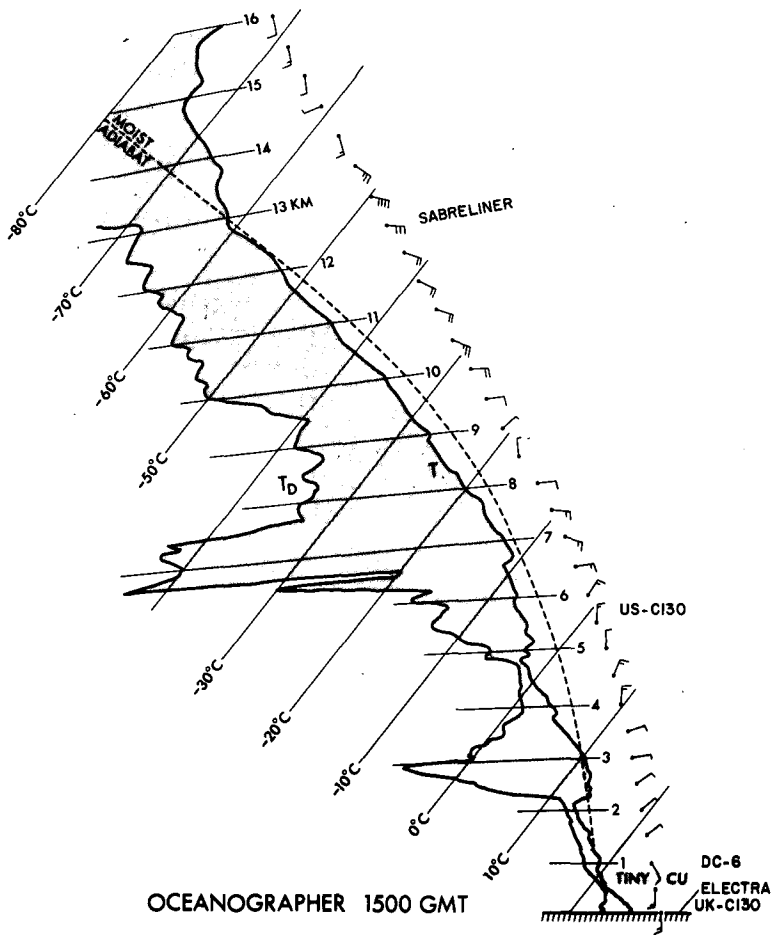

FIG. 2. 1500 GMT. Tephigram from *Oceanographer* situated at 7°44'N, 22°12'W. Solid lines: dew point (T_D) and temperature (T); dashed line: moist adiabat (of constant Rossby's θ_E). Vertical scale is height (km) above the sea. Flight levels of the aircraft are indicated. Winds are shown every 500 m, with one barb = 5 m s^{-1}. Level of tiny cumulus cloud is indicated.

the aircraft is known for any arbitrarily chosen frame, then the cloud position may be plotted on a plan view map. The position of the aircraft was known to a nominal precision of 2–4 km by inertial navigation. The plotting technique was of comparable accuracy (Snow *et al.*, 1975). To find the height of a cloud element, its elevation was measured relative to the horizon; its height then followed from the range. Cloud heights obtained from the C130 side camera agreed to within a few hundred meters with heights derived from an algorithm of Mosher (1975), which yields the height of a cumulus top as a function of visible and infrared brightness seen by satellite. Comparisons are detailed in Table 2. Nominal accuracies in the maps are a few kilometers in the horizontal and ~500 m in the vertical.

At 1437 GMT, while the aircraft were near the southwest corner of the box, the satellite recorded the pattern of visible brightness shown in Fig. 4. Across the east side of the box a cirrus shield was prominent. Isolated bright patches were mostly groups of cumulus, in the southerly anticyclonic flow in the moist layer (Suchman *et al.*, 1977).

The first circuit by the US-C130 was made between about 1341 and 1445 GMT. Prior to this, the aircraft flew across the box, crossing the middle at 1305. The resulting cloud map is presented in two parts. Fig. 3a shows active cumulus tops with heights in the interval 2.5 km to the maximum, exceeding 13 km in the northeast corner of the box. Fig. 3b shows tops below 2.5 km, and the horizontal limits of cirrus anvils. The picture is not complete, particularly of the small clouds, because they were very numerous, and photographic coverage was not obtained simultaneously over the whole area.

Fig. 3a shows relatively few clouds in the southwest part of the box, and more to the northeast, with greater heights. At the time, the cloud cluster was growing in the northeast corner, and propagat-

ing slowly into the box. A cloud with top exceeding 13 km was observed by satellite near D_1. Most cumulus clouds taller than ~3 km tended to be aligned in bands of orientation about 215°, roughly 9 km apart.

Fig. 3b shows that low clouds were arranged differently from the cumulus and cumulonimbus clouds shown in Fig. 3a. A region to the northeast was occupied by bands of altocumulus at 2.9 km, of orientation about 190° and spacing ~3 km.

In the west part of the box, many of the small clouds were arranged in arcs. They were composed of cumulus mediocris sometimes reaching roughly the top of the moist layer (2–3 km). One such arc, obscured from satellite view by a cirrus layer over the north side of the box, has been documented by Warner (1978); this arc is shown in Fig. 5. The clouds leaned backward, in a manner corresponding with winds decreasing with height upward from the top of the mixed layer (Fig. 2). Low-level winds were toward the inside of the arcs.

At the lowest end of the scale of convective motions, there were many tiny cumulus fractus, of linear dimension ~500 m, with bases at about 500–700 m. These were aligned in rows oriented north–south, with separations of 1 or 2 km along and between rows. The rows were aligned approximately with the surface wind. Tiny cumulus also appeared in front of the arcs (Fig. 5).

In connection with the tiny cumulus, Fitzjarrald (1978) has used the *Oceanographer* acoustic sounder data to examine the dominant horizontal scale (l) of free convection in the moist layer. For the period 0827–1225 GMT on day 261, he gave the dominant local period of fluctuation as 6.25 min, the wind speed as 7 m s^{-1}, the depth of the mixed layer (Z_i) as 450 m, and the Monin-Obukhov length (L) as −119 m. The first two numbers yield $l = 2.6$ km, the second that $-Z_i/L = 3.8$. The nondimensional horizontal wavelength $l/Z_i = 5.8$. His Fig. 7 then indicates that this constitutes a relatively low instability, with a relatively large horizontal wavelength. The number 2.6 km corresponds quite well with the spacing of the tiny cumulus along rows shown by the mapping. The information on the rows of tiny cumulus is consistent with the finding of LeMone and Pennell (1976, Fig. 16a) that the rows resulted from forcing below cloud base associated with longitudinal roll circulations, oriented roughly along the wind direction. Tiny cumulus in front of the arc shown in Fig. 5 were aligned parallel to the arc, apparently transverse to the wind direction rather than along it.

With many active towers reaching stable layers, much stratus was present (a feature seen less often in the undisturbed Caribbean). The deep clouds produced anvils at about 13 km (Fig. 3b). Their leading edges spread from slightly south of east at

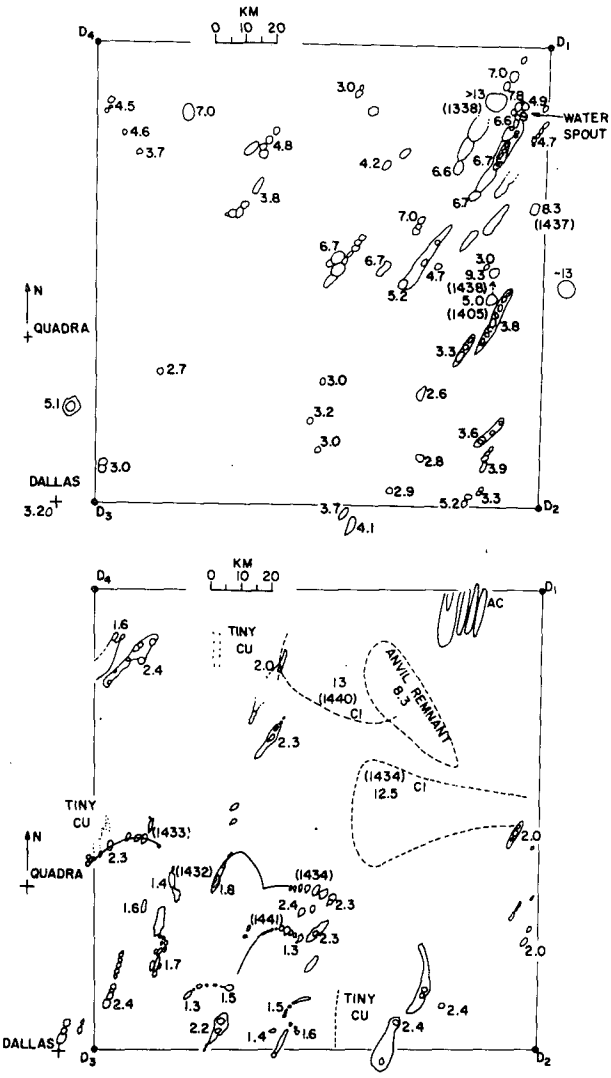

FIG. 3. 1300 to 1445 GMT. a (top): Active tops (outlined by contours) in the height interval 2.5 to >13 km. b (bottom): Clouds of height <2.5 km, and anvils (dashed). Thin solid lines represent arcs of clouds. Numbers are heights (km) above the sea, and times of measurement. The corners D_1 to D_4 define the box circuit (see Table 1).

~25 m s^{-1}. Towers reaching different levels in the troposphere produced individual anvil plumes. An isolated remnant of anvil at 8.5 km was oriented along 145° (rather than ~90° as at 13 km). Many stratus and stratocumulus patches at ~2.5 and 5 km are not portrayed here.

5. Mesoscale patterns seen by satellite, radar and aircraft photography

A 16 mm movie loop of visible satellite images of the boxed area has been made, with time intervals of 15 min. In this movie, it is possible to follow several arc-shaped mesoscale patterns over periods

TABLE 2. Cloud tops by photogrammetry, and cloud tops (and bases) from satellite data by Mosher's (1975) method. (McIDAS is the man-computer interactive data access system at the University of Wisconsin.)

Cloud map position		Height (km)	Time (GMT)	McIDAS position		Top (base)	Time	Comment
8°36′N	21°22′W	~2.5	1407			2.1 (0.2)		Inactive Ac
8°54′	21°23.5′	2.6	1408			1.8 (0.3)	1407	Isolated Cu at end
				8°51.3′N	21°24.9′W	1.9	1422	of dissipated band
9°6.5′	21°10′ to 21°11′	3.8	1352			3.2 (0.6)		High top on Cu band
				9°20.5′	21°34′	4.6 (2.9)	1322	
						4.4 (3.2)	1337	Motion: 3.7 m s^{-1}/030°
9°13′	21°32′ to 21°33′	6.1	1351					Anvil remnant
				9°10′	21°40′		1422	Dissipated
				9°33′	21°9′	10.5	1137	
				9°33′	21°13′	10.0	1152	
				9°34′	21°16′	9.9	1207	
				9°35′	21°17′	9.4	1222	Motion: 4 m s^{-1}/030°
				9°33′	21°15′	8.9	1237	
9°37′	21°28′	8.3	1348					Anvil remnant
9°14.5′	21°3′	13	1349	9°12.1′	21°3.2′	12.2	1352	
9°47′	21°18′	13.1	1336			9.7 (2.5)	1337	
						12.7	1352	
8°58′	21°4′	15	1621	9°16′	21°23′	15.4	1807	Highest towers by each method

exceeding an hour. Three such patterns are shown Figs. 6a–6c. The square box was slightly distorted in the movie, to the shape shown in the figure. It is possible to pick out the positions of these patterns at 1437 in Fig. 4, the visible satellite photograph for that time. The arcs were composed essentially of small clouds, as represented diagrammatically in Fig. 3b.

A frame from the US-C130 nose camera movie at 1428:35 GMT is shown in Fig. 7. The aircraft

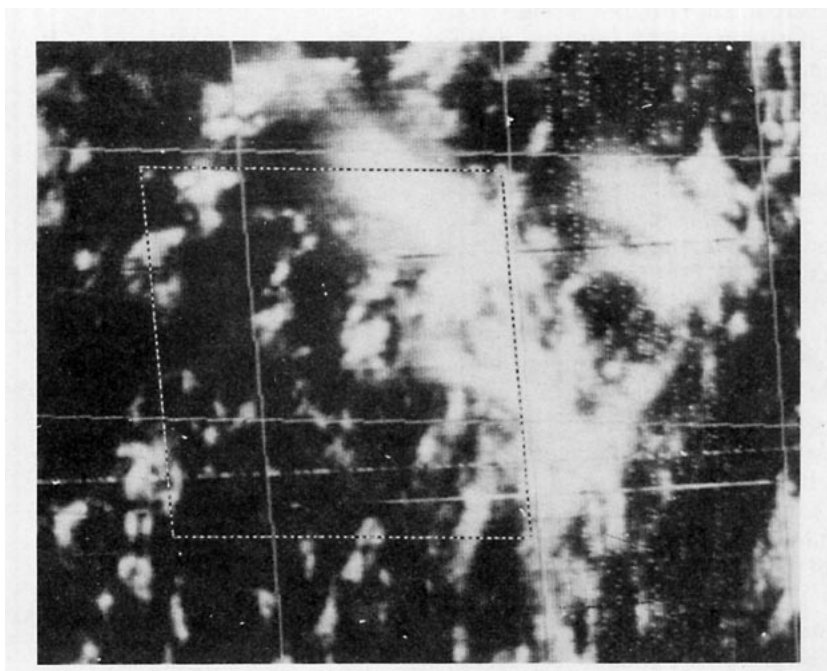

FIG. 4. 1437 GMT. Visible satellite image. The cloud cluster is seen at right center, with anvil cirrus streaming northwestward, north being up the page. The box circuit is shown by pecked lines; a side was 150 km long. Light fiducial lines show the latitudes 9 and 10°N, and longitudes 20, 21 and 22°W.

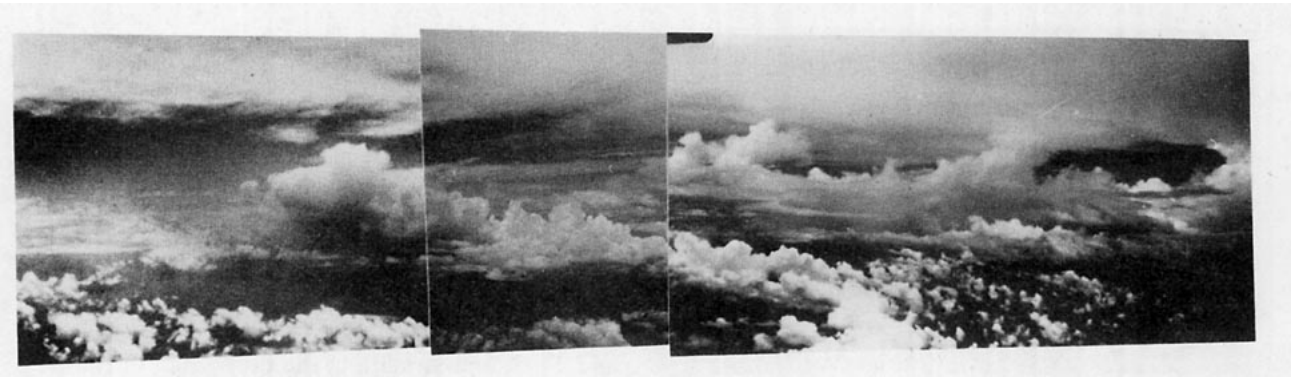

FIG. 5. 1522 GMT. Composite of photographs looking north from the US-C130 aircraft flying at altitude 5.7 km on the north side of the box circuit. High towers of the cloud cluster were to the east and south of the aircraft. Anvil cirrus from them was overhead. In the right foreground is an arc of clouds, moving from roughly the west-southwest (toward the right). Cumulus mediocris in the arc were of maximum height about 2.7 km. They leaned backward. A high tower (at left) reached 9 km. It apparently originated from the arc. Tiny cumulus preceded the arc. Note the evidence of organization in their pattern. Major features have been mapped in Warner (1978).

was flying northward at altitude 6.5 km, coming up on the arc shown in Fig. 6c. The faint diffuse line seen in the satellite view (Fig. 4) is revealed as an arc of cumulus mediocris, preceded by tiny cumulus. From the satellite movie, it was evident that while the arc patterns propagated consistently, their composition continuously changed, with small clouds dissipating and being replaced by new clouds, of lifetime much less than the pattern. Near the west side of the box, the velocity of propagation was from about 198° at 6 m s^{-1}, matching the wind near cloud base. Cloud bases were at 500 m (near the top of the mixed layer) and higher. The pattern velocities measured from the satellite movie loop show that previous estimates from aircraft photogrammetry (Warner *et al.*, 1977) were much too great.

The origins of the arcs and their relationships to

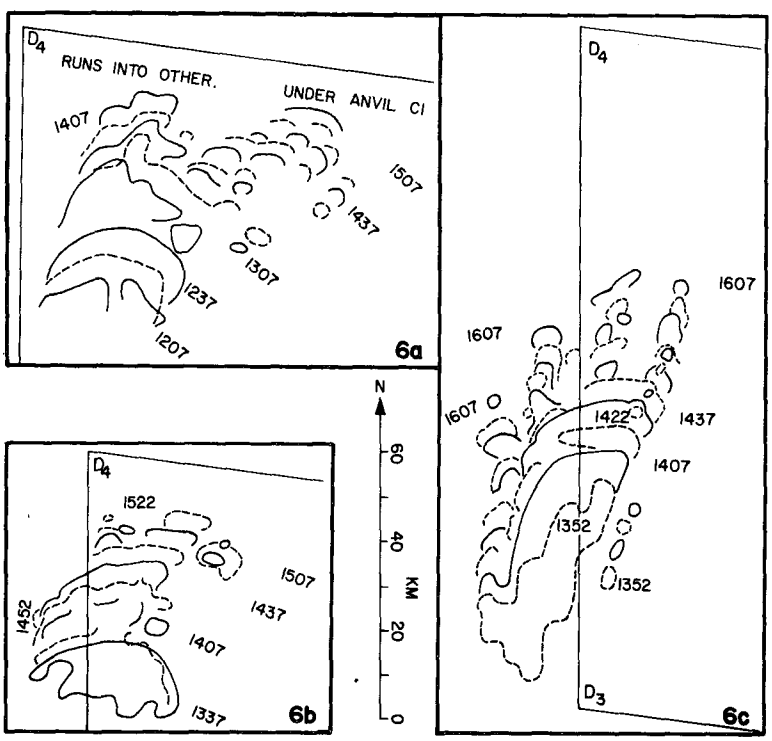

FIG. 6. Motions of arcs traced from satellite movie. The west side D_3 D_4 of the aircraft box circuit is shown. Defined by the latitudes 8°34′ and 9°56′N, and longitudes 21°2′ and 22°23′W, the box was slightly distorted from square shape in the movie.

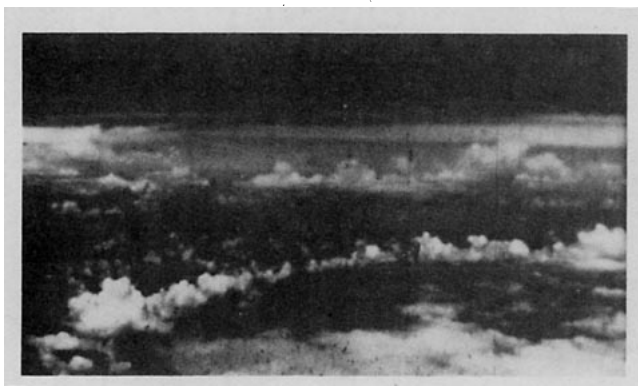

FIG. 7. 1428:35 GMT. Frame from nose camera movie of US-C130 aircraft, taken at altitude 6.5 km while flying northward on the first circuit, coming up on the arc shown in Figs. 6c and 9.

other features were examined. Contour analyses were drawn by hand at an easily discerned threshold of brightness, close to the edge of the visible cloud, seen in projected frames of the movie loops. These maps, at quarter-hour intervals from 1205 to 1435 GMT, appear in Figs. 8 and 9. Superimposed on the contour analyses are alphanumerics representing radar reflectivity, transcribed manually from radar maps as illustrated in Fig. 1 of Warner and Austin (1978). These represent averages over 18 km^2. The relationships between alphanumerics, reflectivity Z and rainfall rate R are shown in Table 3 (for three different expressions for Z, as indicated, the middle column in the table is preferred).

In Figs. 8 and 9, attention is drawn to the arcs in Figs. 6a and 6c, respectively, by small arrows indicating the directions of pattern motion. Occasionally dashed lines appear, where the leading edge of the arcs was marked by faint rather than bright clouds as seen from the satellite. From echo top plan position indicator maps (Warner and Austin, 1978), occasional digits within small squares show peak heights (km) of echo cores. Here a "core" exceeded reflectivity 29 dBZ and occurred within groups of echoes associated with the arcs.

The radar echoes are quite well correlated with the brightness contours. The correlation is not perfect; this is to be expected, because once falling raindrops of size exceeding 0.5 mm and with number densities large enough to yield a radar echo have appeared, small cloud droplet populations are depleted by coalescence or evaporation. It seems from Figs. 8 and 9 that the area of radar averaging (18 km^2) is rather large. Both satellite brightness maps and the radar alphanumerics give rather a coarse view of the activity.

Considering first the arc shown in Figs. 6a and 8, a close association with echoes was apparent until 1235. At 1305 there was bright cloud, but few echoes. More echoes appeared after 1335, with cores often reaching an altitude of 6 km. The persistent arcs were a favored location for generation of new echoes.

The system shown in Figs. 6b and 8 appeared just as a short-lived group of echoes was dissipating. The mesoscale patterns appear to have been generated in association with echoes, and subsequently to have given rise to new clouds and echoes. The same applies to the pattern shown in Figs. 6c and 9.

Attention is drawn to a ring of mean diameter roughly 70 km discernible in Fig. 8 between 1305 and 1405, and straddling the north side of the box. (The north side roughly bisected this feature at 1335.) The arcs of Fig. 6a were on its southwest border. It moved north-northeastward with the low-level flow.

Finally, it may be seen that echoes persisted intermittently near the *Dallas* during the period of Fig. 9. Echo cores reached 4 km. Cloud tops probably reached 5 or 6 km where winds were from the north, rather than from the south as in the mixed layer. Winds averaged through the thickness of such deep clouds were near zero; this probably accounts for the persistence.

The above observations imply that the mesoscale arcs were self-regulating, in a layer near the surface in which winds were from the south-southwest. This corresponds roughly to the lowest kilometer. Precipitation cores extending into the lower middle troposphere apparently generated new mesoscale patterns, and new cores in turn were generated by them.

We may now look from the satellite at a relatively large area, roughly an order of magnitude greater than the area of Fig. 4. Figs. 10a–10c are photographs of intermediate scale at 1422, 1637 and 1825 GMT, respectively. A separate drawing shows corresponding points of reference. Relatively clear air north and west of the cloud cluster is readily seen in Figs. 10; the cluster is toward the lower right in each picture, with cirrus streamers extending northwestward. West and southwest of the cluster, the bands of lower tropospheric clouds represented in Figs. 3a and 4 may be seen. A closer look is necessary to see the lesser clouds like those shown in Figs. 3b, 6 and 7. Much fine tracery is apparent. At 1637 and 1822 arcs were numerous, convex toward roughly the north or northeast, in the direction of winds near the surface. Their radius of curvature was about 20 km, and scale size roughly 40 km.

A comparison of the series of prints in Fig. 10 with the cloud motion fields at 1330 and 1500 GMT by Suchman and Martin (1976), and at 1130 and 1500 by Chatters and Norton (1977), suggested tentatively that the arcs appeared within the moist southerly flow when this exceeded a certain speed, roughly 5 m s^{-1}.

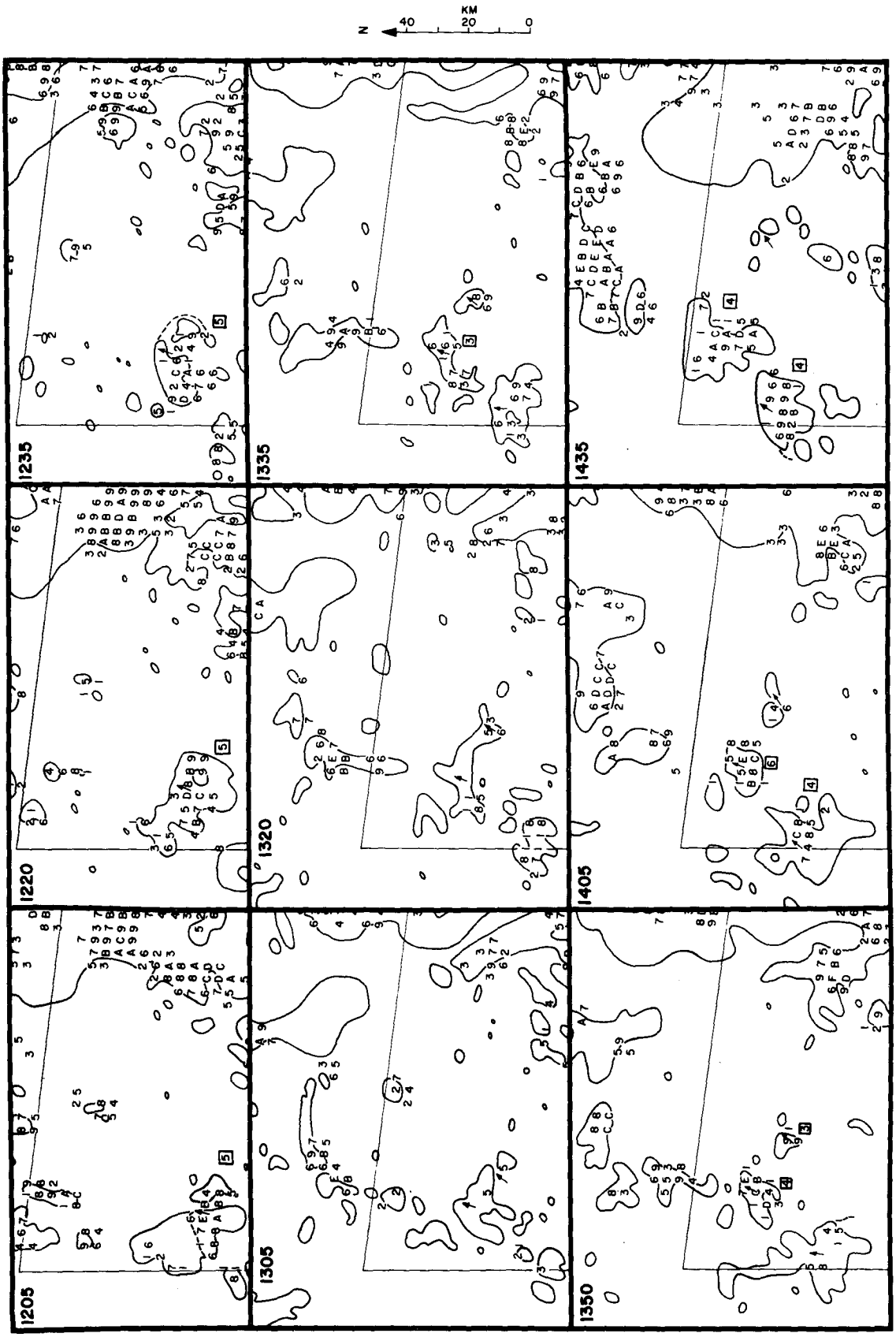

FIG. 8. Maps of visible satellite brightness, together with radar reflectivities in bins measuring 4.2 km north-south by 4.2 km east-west, represented by alphanumerics (see Table 3). Successive times are from 1205 to 1435 GMT at 15 min intervals (two being missing). The satellite and radar scan times differed by 4 min. Radar antenna elevation 0.3°. From echo top plan position indicator maps (Warner and Austin, 1978), occasional digits within small squares show peak heights (km) of echo cores, exceeding reflectivity 29 dBZ, within groups of echoes associated with the arcs. A part of the aircraft box circuit appears in each panel, as in Fig. 6. Solid arrows and dashed lines (indicating a boundary of low brightness) refer to the arc patterns shown in Figs. 6a and 6b.

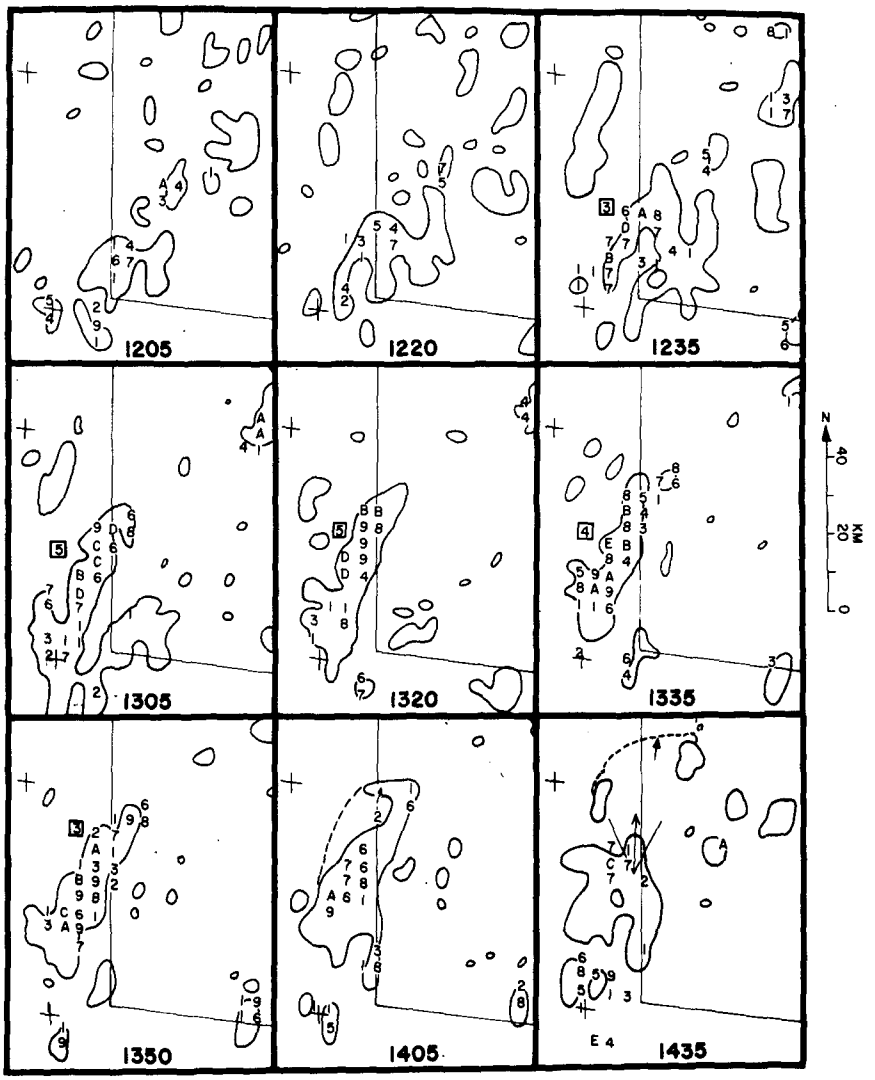

FIG. 9. Maps of visible satellite brightness and radar reflectivities as in Fig. 8. Crosses show the locations of the ships *Quadra* (at 9°3'N, 22°36.5'W) and *Dallas* (at 8°32'N, 22°31'W). Solid arrows and dashed lines refer to the arc pattern shown in Fig. 6c. The photograph Fig. 7 was taken at 1428:35 from an altitude of 6.5 km; the position and field of view are shown with an open arrow in the panel for 1435.

6. Aircraft traverses through mesoscale arc patterns

In this section aircraft data are displayed, which can partly explain how the arcs persisted for up to 2 h, while being composed of elements of individually much shorter lifetimes.

The UK-C130 aircraft flew within the mixed layer, alternately at nominal altitudes of 238 and 52 m, or pressures of 985 and 1007 hPa. The Electra flew just above the mixed layer at nominal altitude 537 m (949 hPa), the DC-6 at 1067 m (891 hPa). The Electra had side-pointing movie cameras with a frame interval of 4 s (~430 m); the DC-6 had a nose camera with a frame interval of 5 s (490 m). From the electra movies, frames were noted for which the aircraft was flying through either clear air, fields of tiny cumulus fractus of linear dimension ~500 m, or fields of cumulus mediocris, or was penetrating a cloud. Using the nose camera on the DC-6, it was possible to do the same analysis, and also to discern the presence of rain.

The DC-6, Electra and UK-C130 flew close to one another in the moist layer during the box circuits. Their recordings of thermodynamic data, made available by NCAR, will be compared for a portion of the first box circuit, from about 1437 GMT, when the aircraft were near the southwest corner D_3, until 1500 GMT, when they reached the northwest corner D_4, the UK-C130 following 25 min behind the other two. They flew northward through the arcs shown

TABLE 3. Radar calibration [from Warner and Austin (1978); column 3 is added from Austin and Geotis (1979)].

Alpha-numeric	Reflectivity (dBZ)	Rainfall rate (mm h^{-1}) from $180\,R^{1.35}$	$170\,R^{1.52}$	$230\,R^{1.25}$
1	11	0.14	0.18	0.098
2	13	0.20	0.24	0.14
3	14	0.23	0.28	0.17
4	16	0.33	0.39	0.25
5	17	0.39	0.45	0.30
6	18.5	0.50	0.56	0.39
7	20	0.65	0.71	0.51
8	22	0.91	0.96	0.74
9	24	1.28	1.29	1.07
A	25.5	1.65	1.62	1.42
B	27.5	2.3	2.2	2.0
C	29	3.0	2.8	2.7
D	30.5	3.9	3.5	3.6
E	33	5.9	5.1	5.6
F	35.5	9.1	7.4	8.9
G	38	13.9	10.8	14.2
H	41	23	17	25
K	44	39	27	43
L	46	55	36	62
M	48	77	49	89

in Figs. 6b and 6c. Time series plots of data from the aircraft, with time running from right to left, are shown in Fig. 11.

Looking in Fig. 11 at temperatures (T) and dew points (T_D) for cases of cloud penetrations, it seems that the aircraft instruments responded well to sudden changes. Effects of rain on temperature measurements—a notorious problem—are not involved here. Penetrated clouds were small; therefore effects of sensor wetting are neglected. At the right of Fig. 11 uncertainty bars for density may be found: an increase in density corresponding to the bars could be caused by changes of −0.2°C in T or −1.2°C in T_D. Changes in plotted densities slightly exceeded those indicated by the uncertainty bars. Potential temperatures fluctuated relatively widely.

During the intervals shown in Fig. 11, the aircraft flew first through the arc shown in Fig. 6c, and then through that shown in Fig. 6b. Using the McIDAS system to superimpose the aircraft track D_3 to D_4 on full resolution visible satellite images at 15 min intervals, the times of passage of the three aircraft through the arcs shown in Figs. 6c and 6b were determined. The arc in Fig. 6c was ~4.5 km wide in the satellite view; cross-hatching in the middle of Fig. 11 indicates its position from the satellite. Cross-hatching near the left of Fig. 11, at later times, likewise shows the passages through the leading edge of the arc shown in Fig. 6b.

Comparing in Fig. 11 the hatched position from the satellite images with the cloud data from the Electra and DC-6 (central strips in the diagram), there is close correspondence between the hatching and the notations C which indicate flight through an environment containing cumulus clouds penetrating through the flight level. This environment is illustrated in Fig. 12, a photograph from the nose camera of the DC-6 at 1448:19 GMT. The notations of cumulus cloudiness (C) show that cumulus convection extended in latitude further than the brightest clouds picked out in the satellite images.

Comparing the notations of cumulus cloudiness and tiny cumulus (C and T in Fig. 11) with the traces of temperature and dew point (T and T_D), it seems that the air of the arcs, containing clouds, featured relatively low temperatures and high dew points at the levels of the DC-6 and the Electra. Near the surface with the UK-C130 such anomalies do not appear at the times of passage of the arcs indicated from the satellite images. Shortly after 1510 GMT the UK-C130 briefly encountered low temperatures and high dew points, with changes of wind. Satellite photographs indicate that probably these phenomena were associated with activity to the south of the arc shown in Fig. 6c.

The arc to the north is relatively difficult to recog-

TABLE 4. Cloud and sounding data from Fig. 11 for arc shown in Fig. 6c (Schematic is shown in Fig. 16). Wind corrections b_v, b_x are from both box circuits. [Lower values are from Grossman's (1977) method.]

Cloud tops		Tiny Cu	Cu med (arc) (~2000 m)	Clear	b_v, b_x (m s^{-1})
Winds at 1067 m	u, v	3.0, 3.5	2.5, 2.8	3.0, 2.0	0.6, 0.3
	m s^{-1} deg^{-1}	4.6/220	3.8/221	3.6/236	(0.5, 0.2)
$-\delta T/\delta z$	(K km^{-1})	5.6	5.8	5.8	
Cloud tops	(m)	~800			
Winds at 537 m	u, v	3.2, 7.6	2.9, 7.3	3.2, 7.0	2.6, −0.1
	m s^{-1} deg^{-1}	8.2/203	7.8/201	7.7/204	(1.7, −0.5)
Cloud bases	(m)	~500	~500		
$-\delta T/\delta z$	(K km^{-1})	~9.0	~9.0	~7.7	
Winds at 238 m	u, v	3.7, 4.5	3.5, 4.2	3.3, 4.8	1.6, −0.1
	m s^{-1} deg^{-1}	5.9/219	5.5/219	5.9/214	(0.5, −0.2)

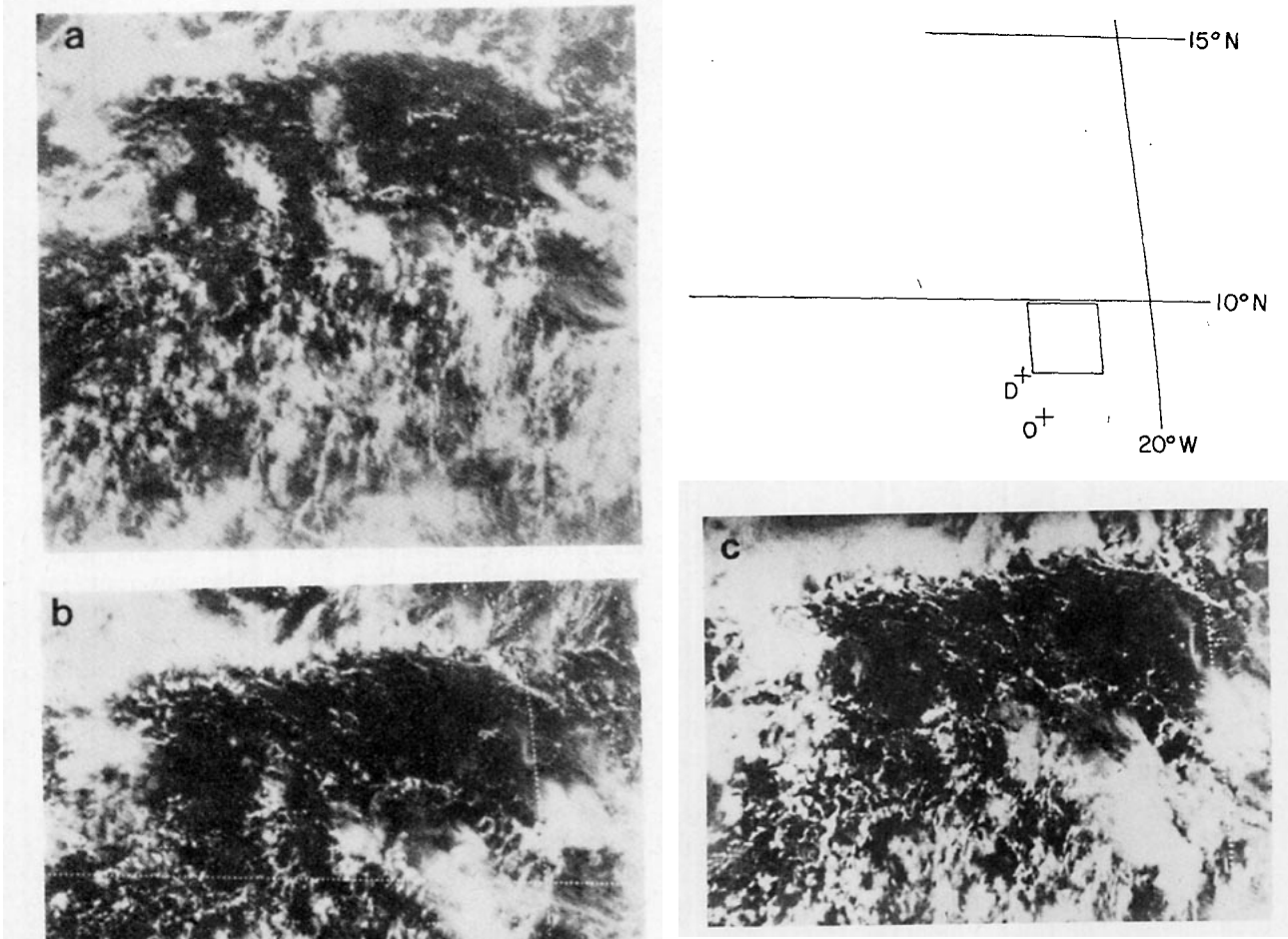

FIG. 10. Visible satellite images (a) 1422, (b) 1637 and (c) 1822 GMT. The drawing shows lines of latitude and longitude recognizable in the photos; also the box circuit, and the approximate locations of the ships *Dallas* (D) and *Oceanographer* (O).

FIG. 11. Time-series plots of data from three aircraft, for the west side of the first box circuit. The plots are keyed to geographical location, shown in the middle. (Note that 0.1° of latitude = 11.1 km.) Cross-hatching indicates the positions of the arcs shown in Figs. 6b and 6c, as derived from full resolution visible satellite images.

At the base is time for the UK-C130. The first plot upward from the base is the density (ρ) of air sampled by the UK-C130 at 15 s intervals, based on 15 s averages (and normalized by transfer to the nominal pressure 985 hPa at constant potential temperature). The next two plots are dew point (T_D) and temperature (T), respectively, plotted every 6 s from 1 s averages (without adjustment for pressure variations). Next come vertical air velocities (W), plotted every 6 s from 6 s averages. Next come winds drawn as short barbs (at 15 s intervals from 15 s averages), after applying the corrections given in Table 4. Winds were from roughly the south: north is upward in this representation of winds; a scale higher up in the diagram on the right shows the length of barb of speed 5 m s^{-1}. The next strip going upward is time for the Electra, then density from the Electra (with normalization to 949 hPa); then T_D, T, W and winds. From the nominal vertical air velocities W from the Electra, a constant 4.6 m s^{-1} has been subtracted. The next strip shows blocks corresponding to times when the Electra was in cloud; above that is a characterization of the convective field through which the aircraft was flying; L means clear air; T (light shading) means that tiny cumulus surrounded the Electra; C (darker shading) means that cumulus mediocris surrounded the aircraft. The central strip in the diagram shows the latitude as the aircraft flew northward at longitude 22.4°W.

The upper middle part of the diagram shows data plotted for the DC-6 in the same manner as for the Electra. The vertical air velocities shown (not available from the NCAR microfilm 1 s data) were abstracted from data over one short flight leg. The mean over the leg may not have been exactly zero, so its removal may mean a (very small) systematic bias.

The DC-6 characterization is slightly different from that of the Electra. The DC-6 flew for much of the time below stratus, and often in mist. In the first strip upward from the middle of the diagram, L means that the air below was clear; T (light shading) means that tiny cumulus were below; C (darker shading) means that cumulus reached 1067 m, flight level. In the second strip, rain (as opposed to the cloud) is indicated by the letter R. Times on the minute when the sky overhead was clear are denoted by L: at other times there was stratus overhead. DC-6 densities were normalized to 891 hPa.

At the top of the figure are plots of virtual potential temperature θ_v and of pseudo-equivalent potential temperature θ_E [calculated by Simpson's (1978) method]. Plots for the different aircraft are superimposed, at 15 s intervals from 15 s averages.

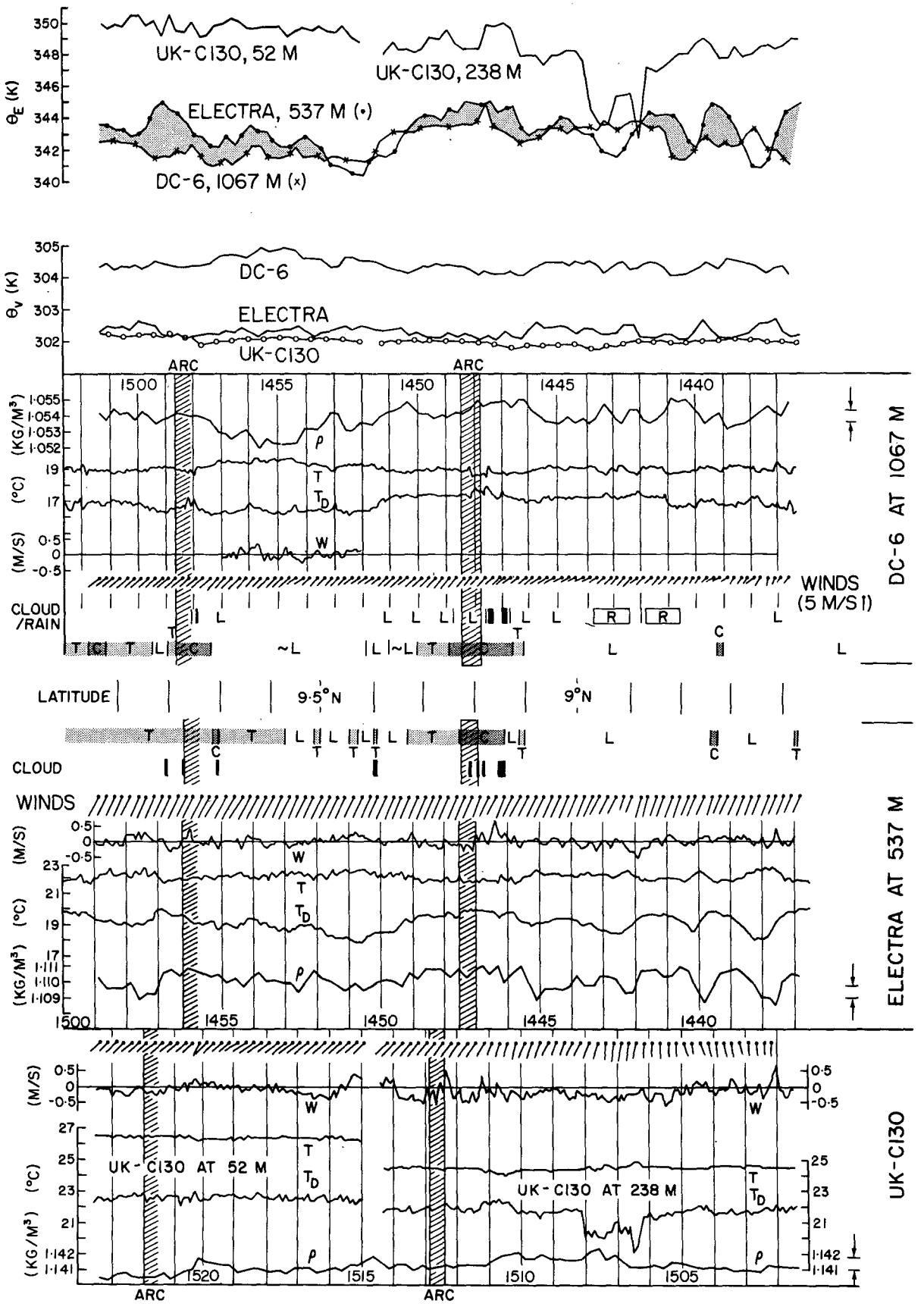
UK-C130, 52 M
UK-C130, 238 M
ELECTRA, 537 M (•)
DC-6, 1067 M (×)
θE (K)
DC-6
ELECTRA
UK-C130
θv (K)
ARC
ARC
1500
1455
1450
1445
1440
ρ
T
TD
W
(KG/M3)
(°C)
(M/S)
CLOUD /RAIN
WINDS (5 M/S I)
DC-6 AT 1067 M
LATITUDE
9·5°N
9°N
CLOUD
WINDS
ELECTRA AT 537 M
UK-C130 AT 52 M
UK-C130 AT 238 M
UK-C130
1520
1515
1510
1505
ARC
ARC

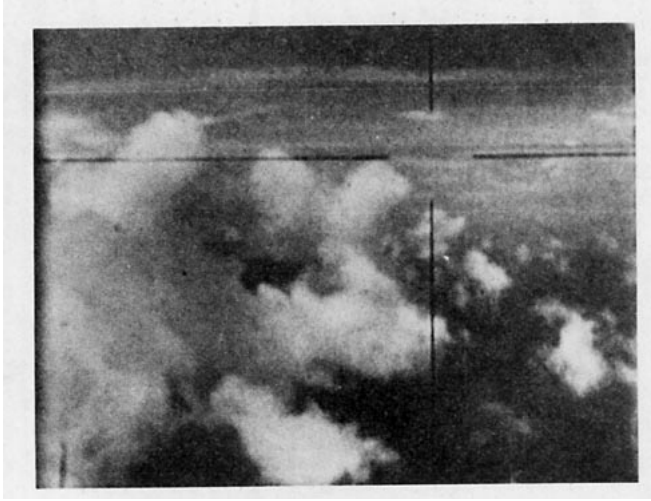

FIG. 12. 1448:19 GMT. Frame from nose camera movie of DC-6 aircraft, taken at altitude about 1067 m while flying northward on the first circuit, within the cumulus environment of the arc shown in Fig. 6c.

nize in Fig. 11. By 1522, when its position was penetrated by the UK-C130, no bright clouds associated with it were present along the aircraft track (see Fig. 6b); it was moving northeastward away from the track and losing its identity.

One other arc was penetrated at low levels, by the Electra flying southward at altitude 35 m at 1612:30 (Fig. 13). As it flew toward the arc, temperatures dropped and dew points rose just as tiny cumulus clouds were encountered. The wind increased and veered (from 6 m s^{-1}/190° to 9.3 m s^{-1}/195°) and then decreased and backed to previous values, within a period of ~1 min or 6 km. This suggests a compact pattern of convergence followed by divergence—of ascent in front with descent (of dense air) behind. The aircraft then ascended from altitude 35 m back up to about 540 m, passing below the base of a vigorous cumulus (at 1614:40), and then entering clear air. This arc was closely associated with precipitating clouds, and the cold gust described may have been associated with precipitation.

Why did the arcs persist for such a long time? First, the traces for the DC-6 and Electra in Fig. 11 show that the environment of clouds of the arcs featured relatively low temperatures and high dew points and air densities. Adjacent clear air featured opposite characteristics, implying that it did not tend to undercut the moist air. Anomalies encountered by the UK-C130 are noteworthy for their absence. (Those at 1507 GMT are discussed below.)

Second, values of θ_v generally increased with height, indicating stability; but it is remarkable that the plots for the UK-C130 and Electra merge in the arcs, indicating neutral stability below cloud base.

Values of θ_E in the arcs decreased with height, indicating convective instability. Weak updrafts (reaching 0.6 m s^{-1}) and downdrafts may be seen in the record from the Electra. On either side of the arcs, above the mixed layer, convective instability decreased to nearly neutral and occasionally stable values. Around the active cumulus of the arcs θ_E was relatively high, probably a result of vertical transport from near the sea. Relatively low absolute values of θ_E on either side of the arc of Fig. 6c, with clear skies (L), high temperatures and low dew points, suggest subsidence.

Third, one may consider air motions in clouds. These generally involve both updrafts and downdrafts on the cloud scale, in adjacent horizontal locations. These cannot readily occur if there is no vertical shear of the wind. With shear, one may visualize updrafts and downdrafts readily coexisting with a circulation having horizontal vorticity (Malkus, 1952). In our case the difference in horizontal wind between the Electra and DC-6 was a few meters per second. Updrafts in the clouds appear to have reached roughly 2 m s^{-1}. It seems that the shear was favorable for the release of instability in small clouds. Fig. 12 shows a close-up view of some of the clouds of the arc of Fig. 6c; individual members of this arc were slender and ephemeral. The clouds appear similar to the small cumuli examined by Telford and Wagner (1974), who found that they moved with a velocity close to that of air near the surface, and featured outward motion near the tops. The clouds seem akin to "hummock" echoes seen by acoustic sounder aboard the *Oceanographer* (Gaynor and Mandics,

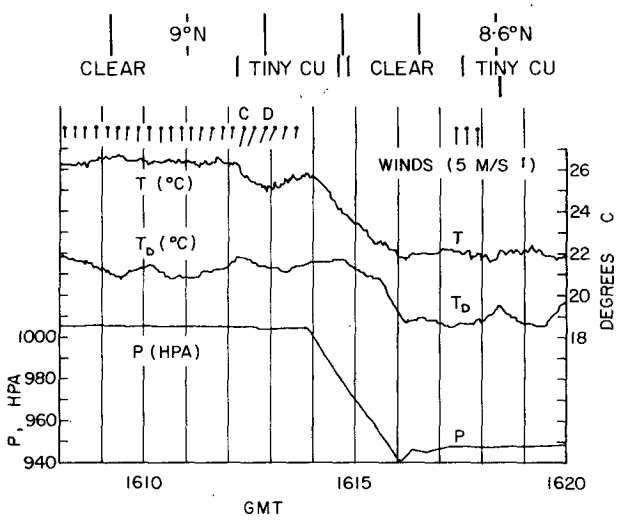

FIG. 13. Time-series plots of data from the Electra, for part of the west side of the second box circuit. At the base is pressure at flight level, then dew points, temperatures and winds plotted in the same way as in Fig. 11. Flight environments of clear air and tiny cumulus are indicated. The Electra flew under the base of a cumulus cloud at about 1614:40 GMT. It penetrated a tiny cumulus at 1618:24. Latitude is shown at the top. Letters C and D next to gusty winds indicate inferred convergence followed by divergence.

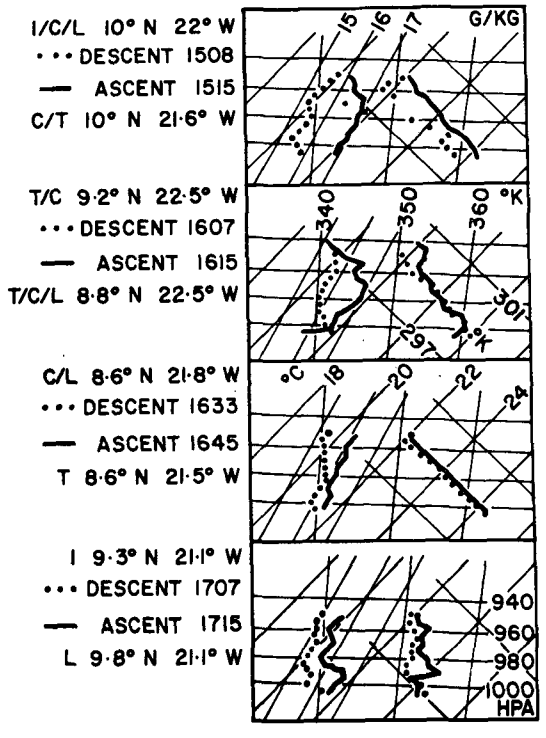

FIG. 14. Soundings from the Electra plotted on Imperial College tephigrams. Isopleths shown of pressure, temperature, specific humidity and dry and pseudo-equivalent potential temperatures. Flight environments, locations and times are indicated (see text for details). See Fig. 4 for locations.

1978). Doppler vertical speed in hummock echoes exceeded 2 m s^{-1}.

Water vapor mixing ratios in the lesser parts of the ranges encountered by each of the three aircraft were compared with rawinsonde and BLIS data (not shown here). These implied that each aircraft encountered air which had subsided from altitudes 500–1000 m above flight level.

Striking in the recordings are the very low dew points and values of θ_E encountered by the UK-C130 at 1507 and 1508, well south of the arc of Fig. 6c. This "dry hole" involved weak descending motion and high densities (although the air was relatively warm). It implies subsidence from a height of several kilometers; apparently a discrete package of air of low θ_E was driven down as a vigorous local return circulation due to a cloudy updraft, and thereafter moved along near the surface. Satellite images show that relatively deep clouds were present near the UK-C130 at this time.

7. Soundings derived from aircraft, and surface conditions

At four times during the two box circuits, the Electra descended from 537 m to 35 m, and returned. Eight soundings were thus obtained, as shown in the tephigrams in Fig. 14. Descents are represented by dots, ascents by continuous lines. The circumstances of the soundings are noted. For instance, "*I/C/L* 10°N 22°W" indicates that the first dotted descent sounding at 1508 GMT was begun in a cloud (I), continued within a field of cumulus mediocris (C), and concluded in clear air (L), near the location 10°N, 22°W (see Fig. 4). The ascent at 1515 started within a field of cumulus mediocris (C) and ended in a field of cumulus (T), roughly 0.4° further east. These soundings indicate that cloudiness was associated with a warm, moist mixed layer, and that clear areas were relatively dry. The last soundings, at 1707 and 1715, were made to the north of the cluster. Its wake was stable.

Conditions in the lowest 10 m above the sea, as assessed from the ship *Dallas*, were broadly undisturbed—meaning an absence of low-lying persistent stable air masses associated with rain. The surface layer did show relatively minor variations associated with small clouds. A singular feature of this day was that the temperatures of the sea, and of the air at 10 m, were alike to within a few tenths of a degree—the measurement uncertainty. Turbulent heat fluxes upward over the lowest 10 m ranged around 70 W m^{-2}, relatively small, and were dominated by the latent rather than sensible heat component.

In order to understand the difference between the regimes of tiny cumulus before the arc shown in Figs. 6c and 11, the arc itself and the clear air behind it, Table 4 is presented. It supplements the data in Fig. 11. The temperature lapse rates ($-\delta T/\delta z$) in the interval 238–537 m were apparently close to but less than adiabatic with the clouds, and stable in the clear air behind the arc. The next 500 m were stable—similar in all cases.

Winds were corrected for systematic overestimates along (b_x) and across (b_y) the direction of flight (see Grossman, 1977). Careful application of Grossman's method for finding b_x and b_y, by choosing turns in relatively undisturbed air, yielded diverse values. On day 261 the aircraft flew around the box circuit first anticyclonically and then cyclonically, so that measurement errors had an equal and opposite effect in the two cases. This allowed choice of b_x and b_y in such a way as to minimize in a least-squares sense the differences in u and in v between the first and second circuits, for each of the four sides of the box circuit. This method seemed to be the best of several alternatives.

Table 4 shows winds typical of the tiny cumulus, the cumulus and the clear air, at the different levels. Wind corrections b_y and b_x are shown at the right of the table. It may be seen that for the Electra and DC-6, application of Grossman's method in the absence of the information from the circuits would have led to u components 1 m s^{-1} less than those

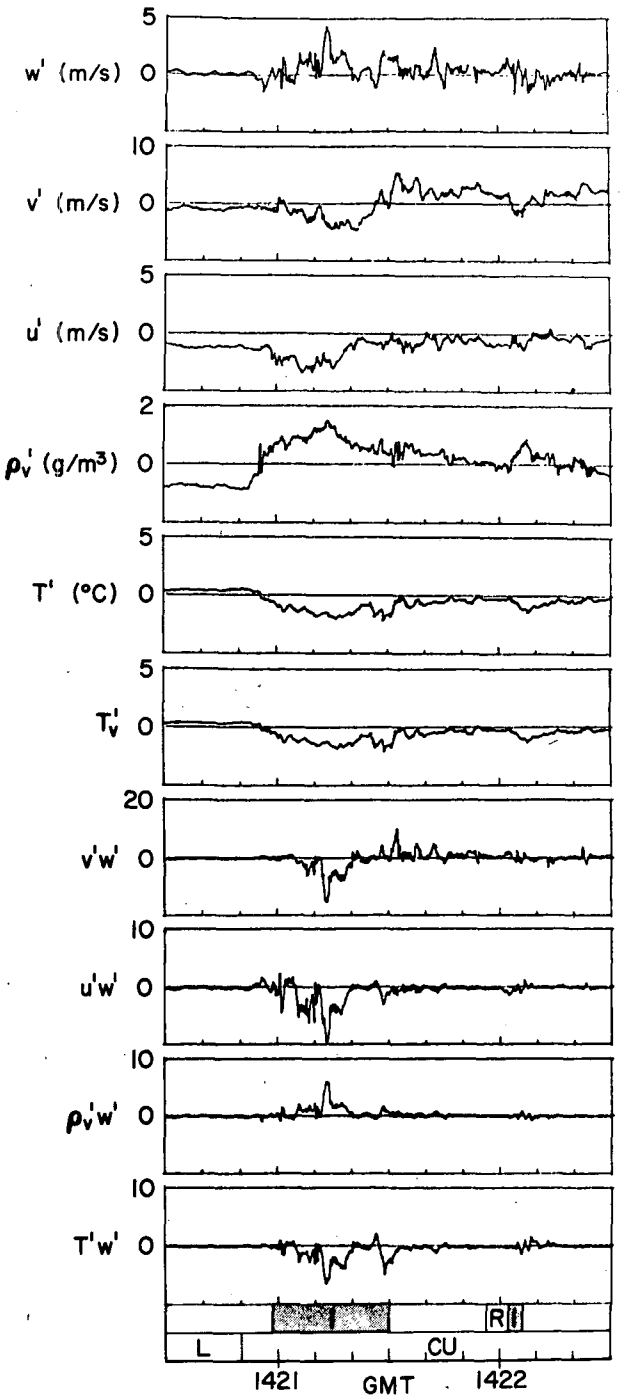

FIG. 15. 1420:30 to 1422:30 GMT. Time-series plots of DC-6 data. From the top: perturbation air speed (m s^{-1}) upward (w'), northward (v') and eastward (u'); water vapor density (g m^{-3}) ρ_v'; temperature T' and virtual temperature T_v' (°C); and fluxes $v'w'$, $u'w'$, $\rho_v'w'$ and $T'w'$. Strips at the bottom show when the DC-6 was in cloud (I) or rain (R), and when it was flying over clear air (L) or among cumulus clouds (CU).

adopted. Such uncertainties limit inferences about the shear of the wind.

It seems safe to conclude that tiny cumulus and cumulus of the arc featured a maximum of wind speed at cloud base (a maximum of v). Perhaps surprising is that wind directions were least at cloud base: a uniform turning with height was expected, but the measurements indicate that this was not the case. That the vertical gradient $\partial u/\partial z < 0$ throughout remains uncertain. The arcs moved from about 198° at 6 m s^{-1} (Section 5). This corresponds with winds near cloud base. Telford and Wagner (1974) found that small cumuli moved at a speed closely related to that of surface air; the present results seem consistent with theirs. Wind speeds decreased in the arcs from front to rear at 537 and 1067 m. This implies vertical confluence into these levels: mesoscale subsidence is inferred, consistent with the speed maximum near cloud base and the stable stratification in the rear of the arcs.

8. Turbulent flux data from aircraft

From the DC-6 aircraft at altitude 1067 m, vertical turbulent fluxes of sensible and latent heat were evaluated. They were means over runs of various lengths, at intervals around both box circuits (Bean *et al.*, 1976). Examining individual traces of perturbation quantities, as in Fig. 15, and comparing these with turbulent fluxes obtained by integration over a total of 35 diverse runs, it was deduced that turbulent fluxes of appreciable magnitude, on the order of hundreds of watts per square meter, were accomplished almost entirely by individual cumulus clouds. All of 18 cloudy updrafts penetrated by the DC-6 during the diverse chosen runs were negatively buoyant. Upward turbulent heat fluxes arose from moist cold updrafts, the moisture being of greater influence than the low temperatures. (Not all cloudy updrafts were measured; those with rain were excluded, owing to deleterious effects on temperature measurements.) The clouds sampled were like those shown in the photograph Fig. 12. They were mostly sampled at an altitude close to their maximum, and were mostly dissipating. Moist cold updrafts near the summits of clouds such as these in the northeast trades were found by Wexler and Malkus (1958). The active stage of a cloud is much briefer than the dissipating stage, so the finding need not be surprising. It is significant here in comparison with findings from the Electra: at 537 m penetrated clouds were roughly neutrally buoyant. The clouds appear to have generated eddy kinetic energy at levels above cloud base but mostly below 1067 m. This is confirmed by weaker updrafts at 1067 m than at 537 m in Fig. 11.

Data from both the DC-6 and the Electra imply that turbulent fluxes in the moist layer are mostly accomplished by cumulus clouds; that mesoscale air circulations were driven primarily by cumulus clouds. The data further lead to the conclusion that the conversion of potential to eddy kinetic energy took place mostly at altitudes between cloud base and 1 km.

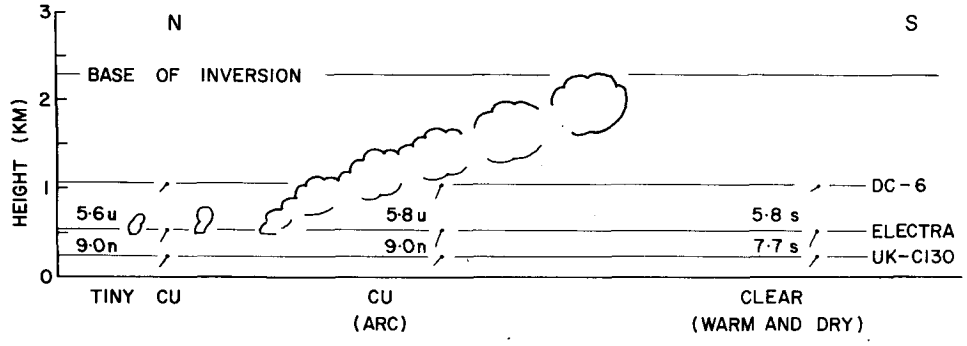

FIG. 16. Schematic diagram of an arc, based on that shown in Figs. 6c and 11. The clouds were composed of a succession of thermals rising in wind shear (see Fig. 5), and have been sketched after the manner of Scorer (1978, pp. 335 and 408). From Table 4, numbers are temperature lapse rates between the levels of flight indicated, and winds are drawn as short barbs as in Fig. 11. From distributions of θ_v and θ_E, the letter S means stable, N neutral, and U convectively unstable. The system moved northward (from right to left). Updrafts occurred at the clouds' leading edges, downdrafts behind. The clear air behind the arc was warm, dry and stably stratified, implying subsidence.

9. Summary and discussion

Conditions of cloudiness in the moist layer, in southerly anticyclonic monsoon flow approaching a growing cloud cluster, have been examined, using airborne and satellite photography, aircraft and ship thermodynamic and wind data, and radar and rawinsonde data.

Unlike middle and upper tropospheric cloud formations, the moist layer featured arc and ring patterns, and rows of small cumulus.

The smallest clouds, called "tiny cumulus", were of linear dimension ~500 m or less; their bases were at 500 to 700 m. These clouds were numerous just in front of arcs of clouds in the moist layer, with separations of 1 or 2 km along and between rows aligned with the wind shear. The data are consistent with a finding of LeMone and Pennell (1976, Fig. 16a) that such clouds resulted from forcing below cloud base associated with roll circulations. Such patterning appeared to occur mostly along the direction of the flow. Also, tiny cumulus were aligned parallel to the arcs, i.e., across the direction of the flow.

The arcs of clouds were very striking. A schematic drawing of one is given in Fig. 16. They were composed of cumulus mediocris reaching roughly the top of the moist layer (2–3 km). Winds near the surface were toward the inside of the arcs. The arcs moved with a velocity close to that of the winds near cloud base. While composed of cumulus mediocris individually short-lived, the patterns persisted for more than an hour traveling steadily. They appeared near radar-detected precipitation. They dissolved finally into patches of cumulus congestus, with radar-detected showers.

Two of the arcs were penetrated by the DC-6 aircraft at 1067 m, the Electra at 537 m and the UK-C130 at 238 and 52 m. At the higher two levels the environment of clouds of the arcs featured low temperatures and high dew points and densities, while clear air on either side of the arcs featured opposite characteristics. There were no anomalies in the mixed layer which could firmly be linked with the arcs shown in Figs. 6b and 6c. One other arc penetrated at altitude 35 m by the Electra showed a convergence-divergence couple involving dense air, of dimension about 6 km; this arc was near radar echoes at the time of sampling.

Virtual potential temperature θ_v increased with height, indicating stability, except between low levels and 537 m in the arcs, where θ_v became about the same at 537 m as in the mixed layer (indicating neutral stability).

Near the clouds, θ_E decreased with height through the aircraft levels, indicating convective instability. In clear air, between 537 and 1067 m, this lapse rate sometimes became stable. The above stability data are tentatively represented by the annotations stable (S), neutral (N) and convectively unstable (U) in Fig. 16.

The arcs in Figs. 6b and 6c featured a wind speed maximum near cloud base (Table 4). Updraft speeds in the clouds appear to have been comparable with the vector difference of horizontal winds through their depth—a condition favorable to overturning. Individual cumulus in the arcs leaned in the direction of the shear—backward with respect to their motion [as shown by Malkus (1952)].

Aircraft measurements of turbulent vertical fluxes showed that they were dominated by cumulus clouds, and that at 1067 m the latent component of the heat flux was generally greater than, and of opposite sign to, the sensible heat component. All the cloud flux data from the DC-6 involved negatively buoyant clouds at 1067 m. (Fluxes were not obtained in large clouds.) The penetrated clouds appeared to be dissipating, near the end of their growing stage, with upward deceleration in the prevailing stable stratification. At 537 m with the

Electra, penetrated clouds were roughly neutrally buoyant. It appears that most of the generation of eddy kinetic energy by clouds of the moist layer occurred below ~1 km.

In view of the longevity of the arcs, an absence of special effects in the records from UK-C130, and the evidence of generation of eddies of kinetic energy by clouds, it seems appropriate to perceive the arcs as self-sustaining entities rather than merely the cloudy manifestations of an original density current.

Schereschewsky (1975, Fig. 1) presents a photograph like some of ours, showing an arc of tilted clouds bordering one side of a circular clear area. Black (1978) shows two arc patterns which he associates with large cumulus clouds. That in his Figs. 9 and 10 may have been similar to the arcs described here. The arc in Black's Fig. 11 is apparently merely a border between a tiny cumulus regime and clear air, a case different from the active arcs of day 261. It is interesting that Black writes: "Sometimes adjacent cumulus cloud arc lines intersect; this produces very strong ascending motions and generates a new cumulonimbus cloud system, which starts the whole process over again." Section 5 provides documentation of a scale-interaction process reminiscent of this.

Lease and Matthews (1978) document a continental cloud arc with coordinated satellite and aircraft measurements. Their observations seem like ours. They interpret them in terms of continued influence of downdraft air following deep convection, rather than in terms of a self-sustaining disturbance. The extensive tropical downdraft documented by Zipser (1969) persisted as a density current until 0710 LT 1 April 1967, but may have yielded a self-sustaining arc of clouds by 1330, judging by the aircraft data and satellite photographs respectively.

Vonder Haar *et al.* (1968) have found many rings of clouds in the tropics, of inside diameter roughly 60 km, containing both shallow and deep convection, and lasting on the order of 10 h. These were usually associated with less recognizably organized clouds. A complete ring was found also in this work (Fig. 8, 1305–1405 GMT). It moved at the same velocity as other moist layer formations. Other rings may be perceived in Fig. 10.

10. Conclusions

The analyses suggest that the moist layer on day 261 was dominated by features of horizontal dimension roughly 40 km and lifetime roughly 2 h. We infer that arc patterns were triggered by dense downdraft air accompanying rainfall. Bearing the pattern of the initial forcing, the arcs persisted. Apparently they were driven by constantly renewed convection, which refreshed the original density current at the surface. Downdrafts of convective scale were shown by vertical air motions measured by the aircraft, and suggested by short-lived variations of horizontal wind near and below cloud base, by vertical changes of wind and by the appearance of the clouds. Downdrafts on the mesoscale behind the arcs were suggested by clear skies, stable stratification and a reduction of wind speed at 537 and 1067 m behind the arc shown in Fig. 6c. The self-perpetuating arcs of the moist layer, with downdrafts on both the cloud and mesoscale, seem similar to the self-perpetuating squall lines of the troposphere, with downdrafts on both the cloud and mesoscale (Zipser, 1977). The moist-layer convection appears to have had a primary role in stirring the layer. Processes driven from the surface appear to have dominated the lowest 500 m; heat transport further upward appears to have been accomplished largely by the arcs—and patterns of deeper clouds. The presence both of horizontal convergence at the surface of 2×10^{-5} s^{-1} (Jalickee and Ropelewski, 1979) and a mixed layer capped by a stable layer (Figs. 2 and 14) may be reconciled in terms of net upward fluxes in clouds and subsidence in mesoscale clear areas.

Triggered by precipitation, the arcs in turn yielded new centers of rain. When the latter appeared, they locally dominated the low levels. Thus there was interaction between convection on the vertical scale of the moist layer with convection on a scale of roughly 6 km. While the arcs of the moist layer were a component of the forcing of showering clouds, probably the number density of the latter was controlled not by the arcs, but by overall conditions of the mid-troposphere.

Acknowledgments. We thank Geoffrey Austin of McGill University for radar data, and Margaret Anne LeMone of NCAR for Electra flux data and helpful comments. R. E. McGavin and R. F. Hartmann, among others of NOAA's Boundary Layer Dynamics Group, contributed to the DC-6 data. Claude Ronne of the Woods Hole Oceanographic Institution helped us with photography. Ron Holle of the National Hurricane and Experimental Meteorology Laboratory assisted in making the cloud maps, with William Snow and Eriberto Varona of the University of Virginia. David R. Fitzjarrald and Gary Barnes assisted us with ship data. Michael Garstang and Mary Morris have given us continual support. We thank Bob Williams at the National Climatic Data Center, Asheville for prompt and cheering provision of data. We thank Colleen Leary for her very thorough and helpful review.

We thank Greg Byrd, Nancy Harrison and Kelly Dolan for help with analyses, and Nancy for much photographic work. Drafting was by Thomas Adams and Jim Hamm, and typing by Sandy Smith and Ginty Kelbe.

Most of this analysis was supported by Grant ATM-74-21701-A02 to the University of Virginia, and Grants ATM-7403466 and ATM-78-05951 to the University of Wisconsin, from the Global Atmospheric Research Program, National Science Foundation, and the U.S. GATE Project Office, National Oceanic and Atmospheric Administration.

REFERENCES

Austin, P. M., and S. G. Geotis, 1979: Raindrop sizes and related parameters for GATE. *J. Appl. Meteor.*, **18**, 569–575.

Bean, B. R., R. O. Gilmer, R. F. Hartmann, R. E. McGavin and R. F. Reinking, 1976: Airborne measurement of vertical boundary layer fluxes of water vapor, sensible heat and momentum during GATE. NOAA Tech. Memo. ERL WMPO-36, 83 pp. [U.S. Govt. Printing Office, No. 1977-779-072].

Black, P. G., 1978: Mesoscale cloud patterns revealed by Apollo-Soyuz photographs. *Bull. Amer. Meteor. Soc.*, **59**, 1409–1419.

Chatters, G. C., and C. C. Norton, 1977: Wind sets for GATE from SMS image cloud tracking. Space Sci. Eng. Center Rep., University of Wisconsin, Madison, 8 pp.*

Fitzjarrald, D. E., 1978: Horizontal scales of motion in atmospheric free convection observed during the GATE experiment. *J. Appl. Meteor.*, **17**, 213–221.

Garstang, M., G. D. Emmitt, G. Barnes, D. Fitzjarrald, E. Tollerud and J. D. Brown, 1977: The U.S. GATE tethered balloon system: A discussion of the measurements. Cloud populations and their interaction with the boundary layer. Tech. Rep. 2, University of Virginia, Charlottesville, 89 pp.**

Gaynor, J. E., and P. A. Mandics, 1978: Analyses of the tropical marine boundary layer during GATE using acoustic sounder data. *Mon. Wea. Rev.*, **106**, 223–232.

Grossman, R. L., 1977: A procedure for the correction of biases in winds measured from aircraft. *J. Appl. Meteor.*, **16**, 654–658.

Jalickee, J. B., and C. F. Ropelewski, 1979: An objective analysis of the boundary-layer thermodynamic structure during GATE. Part I: Method. *Mon. Wea. Rev.*, **107**, 68–76.

Lease, J. C., and D. A. Matthews, 1978: A multi-sensor three-dimensional analysis of a meso-high's development. *Preprints Conf. Cloud Phys. Atmospheric Electricity*, Issaquah, Amer. Meteor. Soc., 483–489.

LeMone, M. A., and W. T. Pennell, 1976: The relationship of the trade wind cumulus distribution to subcloud-layer fluxes and structure. *Mon. Wea. Rev.*, **104**, 524–539.

Malkus, J. S., 1952: The slopes of cumulus clouds in relation to external wind shear. *Quart. J. Roy. Meteor. Soc.*, **78**, 530–542.

Mosher, R. F., 1975: SMS cloud heights. Final Report on NASA Contract NAS5-23296. Space Sci. Eng. Center, University of Wisconsin, Madison, 25 pp.*

Riehl, H., 1954: *Tropical Meteorology*. McGraw-Hill, 392 pp.

Ronne, C., 1959: On a method of cloud measurement from aircraft motion picture films. Unpubl. ms., Ref. No. 59–29, Woods Hole Oceanographic Inst., 13 pp.**

Schereschewsky, P., 1975: Les tourbillons de Bénard dans l'atmosphère; fréquence, diversité, dissymétrie. Cellules ovales isolées. Cellules géantes de brise de mer. Conséquences pour l'environnement. *Comptes Rendus*, **B281**, 205–208.

Scorer, R. S., 1978: *Environmental Aerodynamics*. Ellis Horwood, Chichester, England (see pp. 335 and 408).

Simpson, R. H., 1978: On the computation of equivalent potential temperature. *Mon. Wea. Rev.*, **106**, 124–130.

Snow, J. W., E. C. Varona and J. Simpson, 1975: GATE intercomparisons by cloud imagery. GATE Inform. Bull. No. 8, NCAR, 27–43.

Suchman, D. and D. W. Martin, 1976: Wind sets from SMS images: As assessment of quality for GATE. *J. Appl. Meteor.*, **15**, 1265–1278.

——, D. W. Martin and J. Simpson, 1977: The evolving circulation of an east Atlantic cloud cluster. *Preprints 11th Tech. Conf. Hurricanes and Tropical Meteorology*, Miami Beach, Amer. Meteor. Soc., 333–338.

Telford, J. W., and P. B. Wagner, 1974: The measurement of horizontal air motion near clouds from aircraft. *J. Atmos. Sci.*, **31**, 2066–2080.

Vonder Haar, T., K. Hanson, V. Suomi and U. Shafrir, 1968: Phenomenology of convective ring clouds in the tropics derived from geosynchronous satellite observations. *Proc. Int. Conf. Cloud Physics*, Toronto, WMO, 549–554.

Warner, C., 1978: Photogrammetry from aircraft nose camera movies. *J. Appl. Meteor.*, **17**, 1416–1420.

——, and G. L. Austin, 1978: Statistics of radar echoes on day 261 of GATE. *Mon. Wea. Rev.*, **106**, 983–994.

——, J. Simpson and G. van Helvoirt, 1978: Shallow and deep convection: day 261 of GATE. Cloud populations and their interactions with the boundary layer. Tech. Rep. 4, University of Virginia, Charlottesville, 92 pp.**

——, ——, G. L. Austin, D. Suchman and D. W. Martin, 1977: Visual, radar and satellite aspects of GATE clouds on day 261. *Preprints 11th Tech. Conf. Hurricanes and Tropical Meteorology*, Miami Beach, Amer. Meteor. Soc., 347–354.

——, ——, G. Van Helvoirt, D. W. Martin, D. Suchman and G. L. Austin, 1980: Deep convection on day 261 of GATE. *Mon. Wea. Rev.*, **108** (in press).

Wexler, R., and J. Malkus, 1958: Tropical meteorology, observational studies of tropical clouds: Results of 1956 Caribbean aircraft expedition. Unpubl. ms., Ref. No. 58–46, Woods Hole Oceanographic Inst., 122 pp.**

Zipser, E. J., 1969: The role of organized unsaturated convective downdrafts in the structure and rapid decay of an equatorial disturbance. *J. Appl. Meteor.*, **8**, 799–814.

——, 1977: Mesoscale and convective-scale downdrafts as distinct components of squall-line structure. *Mon. Wea. Rev.*, **105**, 1568–1589.

---

* Available from the Space Science and Engineering Center, University of Wisconsin, 1225 W. Dayton St., Madison 53706.

** Available from the Dept. of Environmental Sciences, University of Virginia, Charlottesville 22903.